Journal of Solid State Electrochemistry (2021) 25:93–104
https://doi.org/10.1007/s10008-020-04537-x

ORIGINAL PAPER

Iron(II) phthalocyanine (FePc) over carbon support for oxygen reduction reaction electrocatalysts operating in alkaline electrolyte

Maida Aysla Costa de Oliveira[1] · Valerio C. A. Ficca[1] · Rohan Gokhale[2] · Carlo Santoro[2,3] · Barbara Mecheri[1] · Alessandra D'Epifanio[1] · Silvia Licoccia[1] · Plamen Atanassov[2,4]

Received: 19 December 2019 / Revised: 19 February 2020 / Accepted: 4 March 2020 / Published online: 14 March 2020

Abstract

In this work, we initially report a detailed advancement in the utilization of metal-N_4 chelate macrocycles in the oxygen reduction reaction (ORR). Then, iron(II) phthalocyanines supported on two different carbon-based supports specifically carbon nanotube and black pearl (carbon spheres) were synthesized and their activities toward ORR in alkaline media were studied. With the help of physical and surface characterization like Raman, BET, XRD, XPS, and electron microscopy analysis, the similarity in surface chemistry and surface area of the materials and the differences in the structure and morphology of the supports were established. This work also brings forth the effect of support properties on the electrocatalytic activity of the materials by a detailed electrochemical analysis using rotating disk electrode in oxygen saturated 0.1 M KOH. Comparison with existing literature on Fe-phthalocyanine supported on diverse carbon support is presented.

Keywords PGM-free catalyst · RRDE · Alkaline media · Morphology

Introduction

The demand for clean energy and sustainable development has necessitated the use of energy generation devices like fuel cells. Fuel cells are promising electrochemical devices for energy production and they have several advantages compared to existing technologies such as (i) higher conversion efficiency compared to diesel/gas engines; (ii) water production is the final product of the reaction; (iii) if hydrogen is produced through electrolysis from renewable energy, the overall production of electricity is sustainable and does not produce greenhouse gases; (iv) utilization of hydrogen and not oil or gas (http://www.fuelcelltoday.com/about-fuel-cells/benefits). Despite deep and profound improvements and enhancement in the fuel cell (FC) technology, especially in the past decade, cost of large-scale deployment of FC systems still remains the largest impediment toward a sustainable energy infrastructure. Particularly in the case of low temperature fuel cells, known also as proton exchange membrane fuel cells (PEMFCs) or alkaline membrane fuel cells (AFCs) depending from the operating pH, a significant reduction of cost is needed in order to largely commercialize the technology.

Recently, the US Department of Energy (DoE) has done a cost analysis on direct hydrogen fuel cell vehicles giving also important outlooks and perspectives. Particularly, considering the cost of the entire system to be 3500 US$ (500,000 units/year), the fuel cell stack is estimated to cost 1531 US$ and the auxiliary part named as balance of plant (BOP, air system, cooling system, water humidifiers and recycling, etc.) instead

Electronic supplementary material The online version of this article (https://doi.org/10.1007/s10008-020-04537-x) contains supplementary material, which is available to authorized users.

✉ Carlo Santoro
carlo.santoro830@gmail.com

✉ Barbara Mecheri
barbara.mecheri@uniroma2.it

✉ Plamen Atanassov
plamen.atanassov@uci.edu

[1] Department of Chemical Science and Technologies, University of Rome Tor Vergata, Via della Ricerca Scientifica, 00133 Rome, Italy

[2] Department of Chemical and Biological Engineering, Center for Micro-Engineered Materials (CMEM), University of New Mexico, Albuquerque, NM 87131, USA

[3] School of Chemical Engineering and Analytical Science, The University of Manchester, Oxford Road, Manchester M13 9PL, UK

[4] Department of Chemical and Biomolecular Engineering, Fuel Cells Research Center, University of California Irvine, Irvine, CA 92697, USA

1969 US$, corresponding to 44% and 56% respectively [1]. The main cost related to the fuel cell stack and the overall fuel cell system is the catalyst and its application with roughly contributing to 948$ to the overall system (27%) [1].

Both anodic and cathodic reactions in low temperature fuel cells are catalyzed by the utilization of platinum or platinum group metal catalysts [2]. The oxygen reduction reaction at the cathode requires a large amount of platinum-based catalyst owing to the sluggish nature of this reaction [3, 4]. Not only platinum is an expensive element but platinum-based catalysts are also prone to instability and poisoning especially in the presence of anions [5–11].

US Department of Energy (DoE) suggested several strategies for reducing the cost using a road map. Considering the 2017 baseline of 45 US$/$kW_{net}$, a further reduction to 40 US$/$kW_{net}$ is expected in 2025 by reducing the cost of the Air CEM Unit cost and the bipolar plates cost [12]. The ultimate goal expected by the US DoE (30 US$/$kW_{net}$) envisions also the reduction of platinum loading and decrease precious metal cost [12]. This indirectly underlines that it is necessary and important to act for reducing the catalyst cost and certainly pursue different pathways for even try substituting platinum with lower cost metal elements.

In the past decade, deep attention has been devoted to the development of platinum group metal-free (PGM-free) catalysts for oxygen reduction reaction [13–15]. These catalysts comprehend transition metals (such as Co, Ni, Mn, Fe, and Cu) that are coordinated with nitrogen (as defect on a graphitic/graphene-like structure or as metal-N_4 macrocycles), nitrogen defects/moieties on a graphitic/graphene-like backbone as well as metal oxides [16]. It was recently shown that a direct 4 e^- occur only in the case of the transition metal coordinated with nitrogen [16]. The latter mechanism is preferred because it is faster and more efficient. A 2x2e^- transfer mechanism can also occur on a single site in which the transition metal is coordinated with nitrogen [16]. On this active site, also the reduction of the peroxide (intermediate of the ORR) can occur [16]. Transition metal oxides are generally very well known for being peroxide reducing catalysts [17]. Transition metal particles or nanoparticles are responsible for the reduction of oxygen to the first intermediate through a 2e^- transfer mechanism [17]. Nitrogen defects/moieties can reduce oxygen to peroxide (pyrollic nitrogen) or operates as peroxide reducing active site (pyridinic nitrogen) [16]. Among PGM-free catalysts, several metal-N_4 chelate macrocycles such as porphyrins and phthalocyanines resemble possible structure that act as efficient active site for ORR [18–20].

In the current work, initially, we report a brief review concerning the state of the art of the utilization of metal-N_4 chelate macrocycles for oxygen reduction reaction. Then, the synthesis of iron(II) phthalocyanine supported on two different carbon morphologies (multi-walled carbon nanotubes and black pearl carbon) is reported. The catalytic materials are analyzed by physical characterization technique (Raman spectroscopy). The electrochemical oxygen reduction catalytic activity of these materials is then studied in alkaline electrolyte by means of rotating ring disk electrode measurements. A discussion on the association and differences of morphology and its impact on electrocatalysis is presented. A critical comparison of the obtained results with existing literature on the interaction of support structure and active catalytic sites is presented.

Advancement in the utilization of metal-N_4 chelate macrocycles for oxygen reduction reaction

Out of the several alternatives for platinum or platinum group metal catalysts that have been experimented and tested, metal-N_4 chelate macrocycles supported on carbon materials are some of the best performing alternatives for the cathodic oxygen reduction reaction in alkaline electrolytes [18]. However, in many cases, the synthesis process is quite tedious and the search for the ideal inexpensive and high-performance catalyst in this class of materials continues. Iron(II) phthalocyanines (FePcs) are an attractive metal-source catalyst due to its unique properties such as centrosymmetric structure and electron-donating ability, thanks to their large conjugated molecular structure and strong interactions between aromatic rings [21, 22]. On the other hand, many investigations have been designed that FePc as catalysts for ORR have poor electron conductivity, stability and are prone to aggregation phenomena, contributing to a decrease of active sites and respectively difficult electron transfer in the ORR process [23–25]. Therefore, to supply these disadvantages, as previously mentioned, a conductive carbon support is needed to improve its electrocatalytic activity.

In a previous study, Zagal et al. have demonstrated different electron transfer mechanisms for oxygen reduction through the electrocatalytic activity of different metallophthalocyanines, including Fe-N_4 adsorbed on oriented pyrolytic graphite (OPG) [26]. Further on, Zagal and co-authors presented a variety of electrochemical reactions involving active catalysts based on metal-N_4 chelate confined on the modified the surface electrodes [27]. Wu and co-collaborators on the other hand add an ionic surfactant on the Fe-N_4 complexes to create an electric field at the electrode double layer and consecutively modulate the oxygen reduction selectivity of Fe-N-C catalysts [28]. Zhang et al. have shown the use of graphitized carbon black as support for iron(II) phthalocyanine (FePc) to tune its electronic properties by the delocalized π-electron cloud. This catalyst exhibited high performance in alkaline fuel cells [29]. Cui et al. have performed extensive studies on the role of FePc supported on graphene in oxygen reduction in alkaline electrolyte [30]. Taniguchi et al. have studied oxygen reduction by

self-assembled structure of FePc on reduced graphene oxide [31]. While Jiang et al. have shown the effects of stabilization and solubilization between reduced graphene oxide and FePc through the π-π interaction. These effects provided more active sites and improved the stability of the catalyst in alkaline media [32]. In previous study, Jiang et al. and Zhang et al. reported nitrogen-doped graphene to support FePc composite as catalyst for oxygen reduction with electrocatalytic activity compared to commercial Pt/C [32, 33]. Recently, high performed composite FePc onto N-doped graphene obtained via electrochemical exfoliation demonstrated good oxygen reduction activity followed by long-term durability in alkaline media. Komba et al. confirmed the best activity of their catalyst in comparison with precious metal Pt/C [34]. Cheng and co-workers, however, have developed a class of ultrafine transition metal oxide (TMO—Fe, Co, and Ni) incorporated with Fe-N_4 macrocycles on graphene. The ultrafine TMO/FePc-based catalysts have shown a high performance for ORR in alkaline ambient, and the enhanced ORR activity is attributed to the effect of synergetic TMO ultrathin assist the oxygen reduction on FePc with graphene substrate [35].

The importance of the specific surface area and surface-active sites of three different carbon matrixes to a uniform dispersion of FePc was shown in the study of Li et al. Here, reduced graphene oxide, mesoporous carbon vesicle, and ordered mesoporous carbon have combined with FePc macrocycle through non-covalent π-π stacking interaction. Ordered mesoporous carbon/FePc displayed best ORR performances in acidic and alkaline media [36]. Liu et al. designed a novel FePc-graphene hybrid obtained by an amination reaction of carboxyl-functionalized graphene and FeTAPc with an exhibited high activity and stability toward ORR displaying a direct 4-electron pathway to water and tolerance to metal crossover in alkaline conditions [37]. Zhang et al. utilized FePc on modified porous graphene via pyrolysis of porous freeze-dried composites. The electrocatalysts exhibit three-dimensional interpenetrated porous structure, with high number of active sites for a direct 4-electron pathway [38]. Ohtsuka and co-workers fabricated FePc embedded in the composite thin film with different mixing ration of the two components. They have demonstrated the understand phenomenon of the adsorption and interactions of organic molecules on the carbon support [39]. Ultrathin FePc self-assembled on reduced graphene oxide has exhibited an excellent catalytic activity superior to precious Pt/C catalysts for an ORR alkaline media. Takaaki Taniguchi et al. suggest that this kinetic behavior is caused by hybrid architecture and its synergistic effects that afforded an ultrafast 4-electron transfer during reduction step [40]. Recently, Qiu et al. revealed a catalyst based on isolated Fe-N_4 single atomic anchored on graphene hollow nanospheres with excellent oxygen reduction performance, long-term stability, and good tolerance to NO_x and SO_2 in basic media [41].

Pyrolysis treatment is usually required to improve the metal-nitrogen complex active sites, stability and structural changes, as consequence increase significantly the ORR activity. These two effects depend on the temperature. Nabae and co-workers demonstrated that FePc supported on carbon after heat treatment at 600 °C maintain Fe-N_4 coordination and very high active sites for oxygen redox in alkaline pH [42]. Miller et al. in its study have focused on the influence of heat treatment (400–1000 °C) on the structure of electrocatalysts based on FePc and Ketjen superconductive carbon black. The active sites of Fe-N_4 annealed at temperature higher than 800 °C have presented a decrease of Fe-N coordination and electrochemical catalytic stability due to the decomposition of FeN_4 structure, while composite treated up to 700 °C were thermally stable [43]. Young et al. have proposed hybrid FePc-carbon nanoribbon catalyst as an efficient oxygen reduction reaction by low temperature process, with higher activity that the current state-of-the-art Pt catalyst in alkaline ambient [44]. Zagal et al. have revisited the correlations between catalytic activity and formal potentials of MN_4 complexes. From the different complexes, Mn and Fe display a 4-electron pathway during the oxygen reduction while Cr and Co involves 2-electron pathway ORR in alkaline media [45]. Additionally, Zuniga and co-workers have tested pyrolysed Fe-N_4 catalysts in pH 13. In this study, they have found a direct relation between Fe(III)/Fe(II) redox transition of the catalysts with the onset potential, indicating that the electrogeneration of Fe(II) from Fe(III)OH^- controls the catalysis during the ORR [46].

Pyrolysis treatment, however, has been widely used as a step in the synthesis process of electrocatalysts based on Fe-N_4 macrocycle as a self-support, avoiding the use of carbon support. Thanks to the composition of these macrocycles (carbon, nitrogen, and transition metal), it is possible to obtain a catalyst containing high active ensembles site density [47, 48]. In this context, Osmieri and co-workers have demonstrated in their study of different pyrolysed M (II)-phthalocyanines (M as Fe, Co, Cy, and Zn) as catalysts for ORR, where Fe was the metal led to the highest catalytic activity with selectivity toward a complete 4-electron reduction to water [49]. Monteverde Videla et al. have studied Fe-N-C catalyst obtained through hard template method from FePc. The performance of the catalyst in a direct methanol fuel cell (DMFC) has pointed that Fe-N-C catalyst displays high methanol tolerance [50]. In succession, Osmieri et al. have demonstrated that Fe-N_4 catalyst is tolerant to ethanol with a promising stability in an alkaline direct ethanol fuel cell (DEFC) device [51].

Single and multi-wall carbon nanotubes (SWCNTs and MWCNTs) offer properties such as large surface area of highly crystallized graphite surface area, in comparison with reduced graphene and carbon black, easily to form a free-standing film and fast oxygen diffusion. These properties are

excellent for FePc deposition, allowing a high stability and control of the catalyst microstructure. Meanwhile, its use has been reduced for FePc-based electrocatalysts, due to the failure to coat Fe-macrocycle on MCWNTs. Based to this point, Yan et al. have shown in their investigation that the oxidation of N-doped MWCTNs have a benefit effect to load more FePc molecules on its surface [52]. Yang et al. have presented a pristine multi-wall carbon nanotube, with highly crystallized graphitic surface, to support iron(II) phthalocyanine hybrid composite with a well-defined nanostructure for an efficient redox of the oxygen in alkaline electrolyte [53]. Dong et al. synthetized FePc coated on single-walled carbon nanotube composite with high properties for the oxygen reduction. The catalyst exhibited an excellent activity than commercial Pt/C and anti-crossover effect for methanol oxidation [54]. Amino-functionalized multi-walled carbon nanotubes (MWCNT-NH_2) modified with FePc display of a great surface area for the reduction of molecular oxygen in basic media, according to Cañete et al. [55]. Years later, in alkaline media, the electrochemical performance of Fe-N_4-macrocycle adsorbed on the edge plane of carbon nanotubes has the same order of magnitude of commercial Pt/C catalysts. Venegas et al. explained that both catalysts own one order of higher surface concentrations of Fe-N_4 complex per geometric area implicate in its possible adsorption contributing for an increasing overpotential ORR [56].

As above mentioned, many studies were concentrated on the catalytic activity of Fe-N_4 complex because its crucial role for the ORR from the iron redox couple. However, FePc plays a pivotal role also with respect to the nitrogen content as a precursor source. In fact, by using MN_4 nitrogen content and Fe-Nx species can be easily controlled and reach high levels [57, 58]. Nitrogen-dopant in various structural configurations (e.g., pyrrolic, pyridinic, graphitic) can improve the conductivity of hybrid carbon, determining its electronic features, as an electron on the valence shell [59]. Yang et al. have studied the effect of N-doped platelet ordered mesoporous carbon using FePc as a single nitrogen precursor, indicating that the role of Fe in the structure of N-doped catalysts cannot be responsible only for enhancing the ORR, but also for creating more active sites and increase the electrical conductivity [60]. So that, Fe-N-C catalysts can be developed via thermal treatment of FePc supported on a variety of carbon materials. In agreement, Zhang et al. selected FePc/Pc macrocycles with graphitized carbon black as carbon support, to demonstrate a superior ORR via the delocalized π-coordination environment in FePc. In addition, the phthalocyanine of the composite was fundamental to tune the coordination of Fe during pyrolysis, even as Fe dispersion in porous carbon support [61].

Pyrolyzed FePc-coated activated carbon (AC) was prepared by Liu et al. By using evaporation-induced method self-assembly, the Fe-N-AC catalyst exhibits enhanced oxygen redox catalytic activity, owing the high content of nitrogen and iron in its composition, beyond high surface area, porosity, and crystalline structure [62]. Since then, other investigations have been demonstrating that nitrogen and iron content and species are highly influent on the base of catalytic activity of Fe-N_4 on the modified carbon materials as ORR catalysts [63, 64]. Zhang and co-authors have shown a high-performance 3D hierarchical Fe-N-C catalyst composed via a combination of structured porous carbon framework with unsubstituted Pc/FePc complexes. The authors attributed high activity of this material to the well-defined dispersion of Fe on the 3D carbon support [65].

Ao et al. have demonstrated that Fe/N-functionalized three-dimensional (3D) porous carbon networks as a high performed and high durability catalyst toward oxygen reduction in alkaline media. Their pyrolysed electrocatalysts have shown an activity comparable and superior to most Fe-N-C catalysts reported to date [66]. Recent studies have elucidated the correlations between structure-property and the nature of active sites of catalysts toward oxygen redox by using controlled catalyst synthesis for developing advanced single-metal-site catalysts. In this way, Chen et al. have studied extensively for the synthesis of 3D electrocatalysts based on Fe-N-C obtained by zeolitic imidazolate frameworks (ZIFs), as a subfamily of metal-organic frameworks (MOFs). In this study, they proposed a material with high surface area, porosity, and single-metal-site catalyst [67], while Zhang and co-workers provide a recent and innovative 3D frame network from the unique and well-defined MOF precursors. These advanced catalysts can avoid the degradation phenomena of metal due to 3D structure isolate and anchor single metal atom effectively into a hydrocarbon complex [68]. As mentioned by Huang et al., the uses of high-temperature pyrolysis of MOFs produce not only conductive carbon but also contribute to agglomerations of the N-doped porous carbon matrix. In this view, they have proposed a MOFs-based route by using in situ "two-step' annealing to fabricate Fe-N-C with numerous active sites [69].

In a recent study, Jiao et al. have demonstrated Fe-N_4-MOF electrocatalysts developed via single atom catalysts (SACs) multiscale control, with excellent performance in terms of fast oxygen diffusion and electron transfer in alkaline media [70]. Wang and co-authors developed a FePc encapsulated into the zeolitic imidazolate frameworks (ZIFs) catalyst with high active sites for the ORR [71]. A robust triple-component electrocatalyst composed by FePc and platinum nanoparticles (Pt NPs) onto reduced graphene oxide was fabricated to evaluation of oxygen reduction in potassium hydroxide (KOH) aqueous electrolyte [72]. Reio et al. in their recent research revealed the applicability of new catalysts based on metal-N_4 macrocyclic compounds supported on an innovative carbide-derivate carbons (CDCs) as a support for metal-N_4 macrocyclic compounds. Moreover, CDCs are a porous carbon with very high and tenable surface area, establishing a key role for electrochemical performance [73]. Theoretical studies on

FePc systems have been performed to study their catalytic activities by Seo et al. and Mussell et al. [74, 75]. Chemical tuning of FePc systems on carbon nanotubes to afford additional stability was done by the Cho group [76]. De la Torre et al. have demonstrated insight into interaction and control over the spin state of Fe single atom in the FePc complex by its positioning on N-doped carbon support [77]. Furthermore, there are other groups who have studied the catalytic performance of these systems in oxygen reduction reactions [78, 79]. Different factors are known to affect the catalytic activity of such materials ranging from nature and morphology of the carbon support, interaction between the active molecule and support and the nature of active sites.

Experimental section

Synthesis

Synthesis of the catalysts Fe-BP(N) and Fe-CNT(N) was done as described in our previous article [80]. Particularly, initially, the carbon support based on multi-walled carbon nanotubes (CNTs, Sigma Aldrich), and black pearls 2000 (BP, Cabot Corporation) passed through a nitrogen doping procedure consisting in two consecutive treatment. The first step was based on a reflux treatment with concentrated HNO_3 (65 wt%) at a temperature of 90 °C for a total time of 16 h. After this treatment, the material passed through fine filtration and washing procedure for neutralizing the pH. The obtained powder was then dried (70 °C overnight) and manually ground with a mortar and a pestle. The second step of nitrogen doping procedure consisted into a heat treatment at controlled temperature of 400 °C (5 °C min^{-1} heating ramp) for an amount of time equal to 4 h. The obtained CNT(N) and BP(N) had a BET surface area of 359 and 1317 $m^2\ g^{-1}$, respectively. After the procedure of nitrogen doping, iron(II) phthalocyanine (FePc), purchased from Sigma-Aldrich, was deposited onto the carbon support. Equal quantity (0.5 g) of FePc and CNT(N) or BP(N) were dispersed within 30 mL of methanol used as solvent. The mixture was subject to stirring for 30 min into a water bath keep at constant temperature of 70 °C in order to allow methanol evaporation. After this operation, the powder was fully dried at 70 °C for 3 h. The obtained powders were named as Fe-CNT(N) and Fe-BP(N) depending from the carbon support utilized. The BET surface area of Fe-CNT(N) and Fe-BP(N) are observed to be 112 and 115 $m^2\ g^{-1}$, respectively.

Characterization

The catalyst surface morphology was investigated using scanning electron microscopy (SEM) and transmission electron microscopy (TEM). SEM images were takes through Hitachi S-800 instrument at different magnification. Transmission electron microscopy (TEM) imaging was carried out on a JEOL 2010 instrument on a copper grid. The XPS spectra were measured and described in a previous work [80].

Electrochemical measurements

The catalyst ink was prepared by mixing 5 mg of the catalyst with 150 μL of 0.5 wt% Nafion solution (FuelCellStore, USA) and 850 μL of DI: IPA 1:1 ratio. This mixture was then sonicated in order to obtain a uniform dispersion. Ten microliters of the ink was drop cast on the glass carbon disk of the working electrode (3 times). The loading obtained for each catalyst was 0.6 mg cm^{-2}. The electrolyte used was either N_2- or O_2-saturated 0.1 M KOH. The reference electrode used was Hg/HgO calibrated against RHE. Cyclic voltammograms were recorded from 0 to 1.0 V vs. RHE at a scan rate of 5 mVs^{-1}. The double-layer capacitance was calculated by integrating the voltammetric double-layer (CV in N_2-saturated electrolyte) over a one-volt-wide potential range [81, 82]. ORR activity was evaluated by linear sweep voltammetry from 1.0 to 0 V vs. RHE, using 5 mVs^{-1} potential scan rate. The electrode rotation rate was 1600 rpm. The ORR kinetic current density (J_k) was determined from the Koutecky-Levich equation at 0.9 V, removing background current and normalizing to the electrode geometric area [83]. The RRDE setup is used to measure the current density produced by the disk (J_{disk}) but also the current density of the ring (J_{ring}) to quantify the intermediate (HO_2^-) produced during the ORR. N is the collection efficiency (0.37). The percentage peroxide generated was calculated from the following Eq. (1):

$$\%H_2O_2 = \frac{200 \times \frac{I_{ring}}{N}}{I_{disk} + \frac{I_{ring}}{N}} \tag{1}$$

The number of electrons transferred (n) is a good indicator of ORR reaction mechanism. It is calculated by Eq. (2):

$$n = \frac{4 \times I_{disk}}{I_{disk} + \frac{I_{ring}}{N}} \tag{2}$$

Results and discussion

The morphology of these FePc-based catalysts was observed by electron microscopy techniques (Fig. 1). Scanning electron microscopy (SEM) image (Fig. 1a) of Fe-BP(N) catalyst demonstrates the micrometer sized agglomerations which is further explored by the transmission electron microscopy (TEM) image (Fig. 1c) at high resolution, that confirms the presence

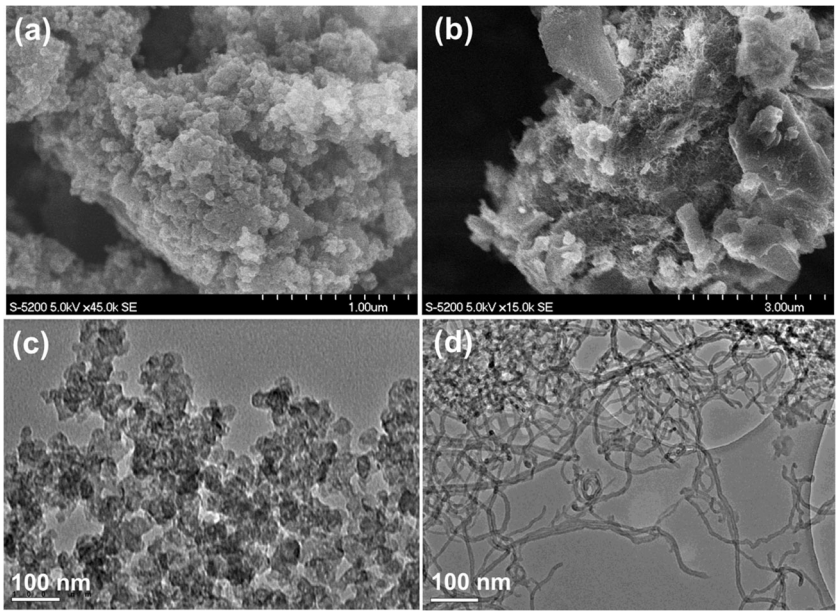

Fig. 1 SEM images showing morphology of **a** Fe-BP(N) and **b** Fe-CNT(N); TEM images showing the nanostructure of **c** Fe-BP(N) and **d** Fe-CNT(N)

of spherical carbon nanoparticles (in the size range of 10–50 nm). The presence of dark areas on the TEM image indicates the presence of iron component of the catalyst. The multi-walled carbon nanotube based catalyst Fe-CNT(N) exhibits a different morphology as compared to the black pearls based catalyst. The lower resolution SEM image of Fe-CNT(N) (Fig. 1b) demonstrates the presence of nanotubes in larger crystallites. The higher resolution TEM image (Fig. 1d) reveals the structure and agglomeration of the carbon nanotube support in the Fe-CNT(N) catalyst. Again, the darker region represents presence of iron containing species. As mentioned before, BET surface area of Fe-BP(N) and Fe-CNT(N) are observed to be ~ 115 and 112 m^2g^{-1} respectively. Since the surface area of these catalysts is similar, the differences in catalytic activity cannot be attributed to this factor. The X-ray diffraction (XRD) pattern of the samples shows the characteristic carbon peaks (Fig. 2a). The Fe-CNT(N) and Fe-BP(N), both exhibit a prominent 002 graphitic peak at 2θ value of 26.2. The Fe-CNT(N) and Fe-BP(N), a 101 peak at 2θ value of ~ 43.4 and 43.7, respectively. In addition to the carbon content, additional peaks are exhibited at $2\theta = 18.2$, 23.8, 26.2, and 30.4 in Fe-BP(N) and $2\theta = 18.2$ in Fe-CNT(N). These peaks result from the metallic content of these catalysts.

Raman spectroscopic analysis of the morphology (Fig. 2b) reveals interesting details of the surface properties of these catalysts. The characteristic carbon peaks D and G appear at 1353 cm^{-1} and 1593 cm^{-1} respectively along with a 2D peak at 2686 cm^{-1} for both the catalysts [80]. The ID:IG ratio (ratio of peak intensity), which reflects on the defect density of these materials, is different. The ID:IG ratio for Fe-BP(N) is ~ 1.04 indicating a higher defect concentration as compared to Fe-CNT(N), which has a value of ~ 0.73. Since the amount of active catalyst is similar in both cases, it can be safely assumed that this difference arises due to structure of the support. Clearly, the black pearl carbon support possesses higher

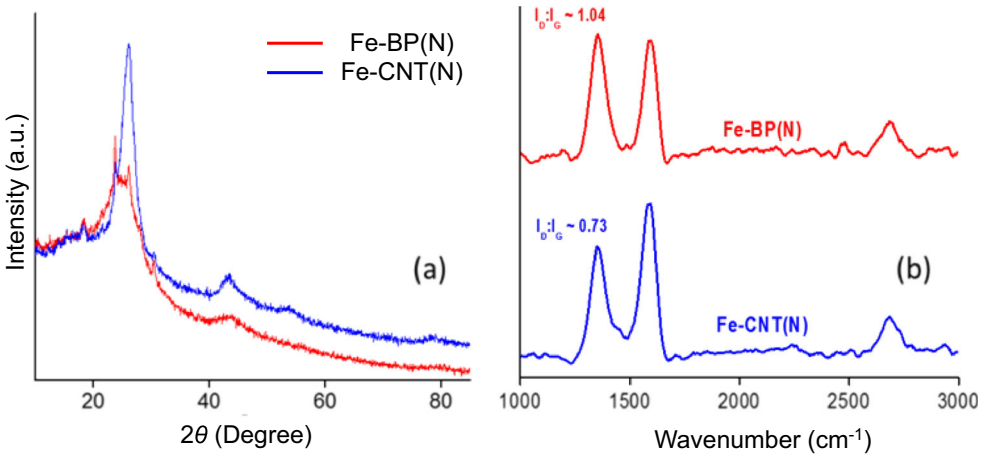

Fig. 2 **a** XRD and **b** Raman spectroscopy for the catalysts

defects because of the decreased graphitization and spherical morphology. The carbon nanotubes on the other hand are highly conducting with less number of defect sites. The defects in Fe-BP(N) can contribute to the catalytic activity as does the better electron conductivity of carbon nanotubes in Fe-CNT(N) [84, 85]. XPS results are discussed in detail in our previous article and correlated to oxygen reduction in neutral medium. It is clearly observed that the N content in Fe-BP(N) and Fe-CNT(N) is 5.8 at% and 10.0 at% and the carbon content ranges from 79 to 82 at% [80]. It has been previously established that pyridinic nitrogen and nitrogen coordinated to Fe sites contribute most efficiently to the 4-electron reduction of oxygen [16]. The pyridinic N content in Fe-BP(N) and Fe-CNT(N) is 62.2 and 47.4 at%, respectively [80]. Furthermore, the N-Fe content of Fe-BP(N) and Fe-CNT(N) is 26.7 and 28.3 at%, respectively.

The remarkably high content of pyridinic and N-Fe content of the catalysts Fe-BP(N) and Fe-CNT(N) contributes to their high oxygen reduction catalytic activity in alkaline electrolyte. The catalysts also show a high percentage of Fe content of which the Fe-N active sites form a major part. This overall surface chemistry significantly enhances the ORR catalysis of the materials under study.

Figure 3 shows cyclic voltammograms of Fe-BP(N) and Fe-CNT(N) (Fig. 3a and c) together with those of bare BP(N) (Fig. 3b and d) in either O_2- and N_2-saturated alkaline electrolyte (0.1 M KOH). While no faradic peaks were detected under N_2 purging for both BP(N) and CNT(N), the weak and broad redox peaks just detectable at 0.8 V for Fe-BP(N) and Fe-CNT(N) are associated with the Fe(III)/Fe(II) redox transition of the metal macrocycle [84]. When the electrolyte is saturated with oxygen, all samples showed a well-defined reduction peak, indicating the oxygen reduction catalysis of both Fe-based catalysts and bare carbon supports. In particular, the deposition of FePc on carbon supports results in a positive shift of the oxygen reduction potential and in an increase of peak current density with respect to bare BP(N) and CNT(N).

From the data collected, it can be seen that iron phthalocyanine alone is the catalytically active species while the role of the supports is for transporting electrons and providing larger surface area for deposition of catalytic sites. The electrochemical surface area (ECSA) was obtained by integrating CV curves (N_2 atmosphere)

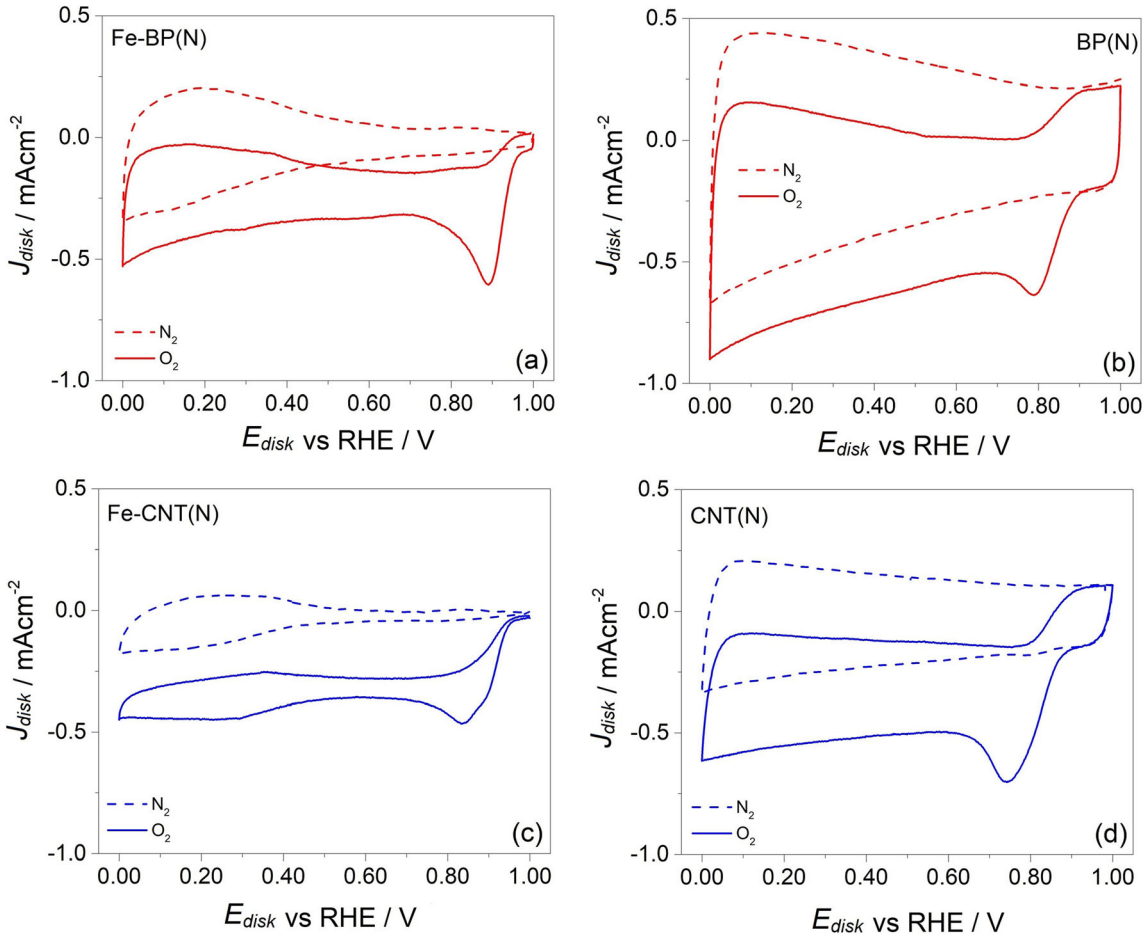

Fig. 3 Cyclic voltammograms for Fe-BP(N) (**a**), BP(N) (**b**), Fe-CNT(N) (**c**), and CNT(N) (**d**) in N_2- (dashed line) and O_2-saturated (solid line) 0.1 M KOH (scan rate 5 mVs^{-1})

in Fig. 3, resulting to be 1055 m^2g^{-1} (BP(N)), 57 m^2g^{-1} Fe-BP(N), 553 m^2g^{-1} (CNT(N)), 45 m^2g^{-1} for Fe-CNT(N). As expected, those values are lower than BET surface area values.

To get deeper insights on ORR activity and mechanism at the surface of Fe-based catalysts, RRDE experiments were carried out. Linear sweep voltammetry (Fig. 4a, both cathodic and anodic trace) shows the oxygen reduction catalysis of Fe-CNT(N) and Fe-BP(N) in O_2-saturated alkaline electrolyte. The onset potential (~ 0.95 V vs RHE) and the half-wave potential (~ 0.84 V vs RHE) are similar for both catalysts because of the similar iron phthalocyanine based active sites. Nevertheless, the impact of different substrates is appreciable in terms of diffusion limited current density (J_d) and kinetic current density (J_k); in fact, J_d was 6.12 $mAcm^{-2}$ and 5.37 $mAcm^{-2}$, while J_k was 1.26 $mAcm^{-2}$ and 0.835 $mAcm^{-2}$ for Fe-BP(N) and Fe-CNT(N), respectively. LSVs were also done in N_2-saturated electrolyte showing practically no activity. LSVs were also run for BP(N) and CNT(N) and presented in Figure S1. These curves showed much lower electrocatalytic activity toward ORR compared to the catalysts supporting Fe-Pc.

The peroxide percentage calculated from the ring current observed in the RRDE measurements is found to be in the low range of 2–3% for both the catalysts (Fig. 4b). Oxygen reduction process is known to follow either 2-electron kinetics that generates hydrogen peroxide as the product or the 4-electron process, which generates water as the product. The latter is the preferred mechanism because it yields more current per molecule of hydrogen making it more efficient and also due to the fact that peroxide is a catalytic poisons which affects the catalyst durability. The number of electrons is calculated using the disk and ring currents in the RRDE measurements (Fig. 4c). It is clear that the ORR process on both the catalysts is close to the ideal 4-electron transfer process, making them efficient catalysts.

Discussion and comparison with existing literature

As previously argued, two Fe-N-C-based electrocatalysts obtained from iron(II) phthalocyanine (FePc) supported onto two different carbonaceous supports: (i) carbon black pearls (BP) with spherical morphology and high structural defects and (ii) carbon nanotubes (CTN) with channel morphology and high conductivity. The non-pyrolysed catalysts have shown promising catalytic activity toward oxygen reaction reduction in alkaline media comparable with FePc-based catalysts existing in literature.

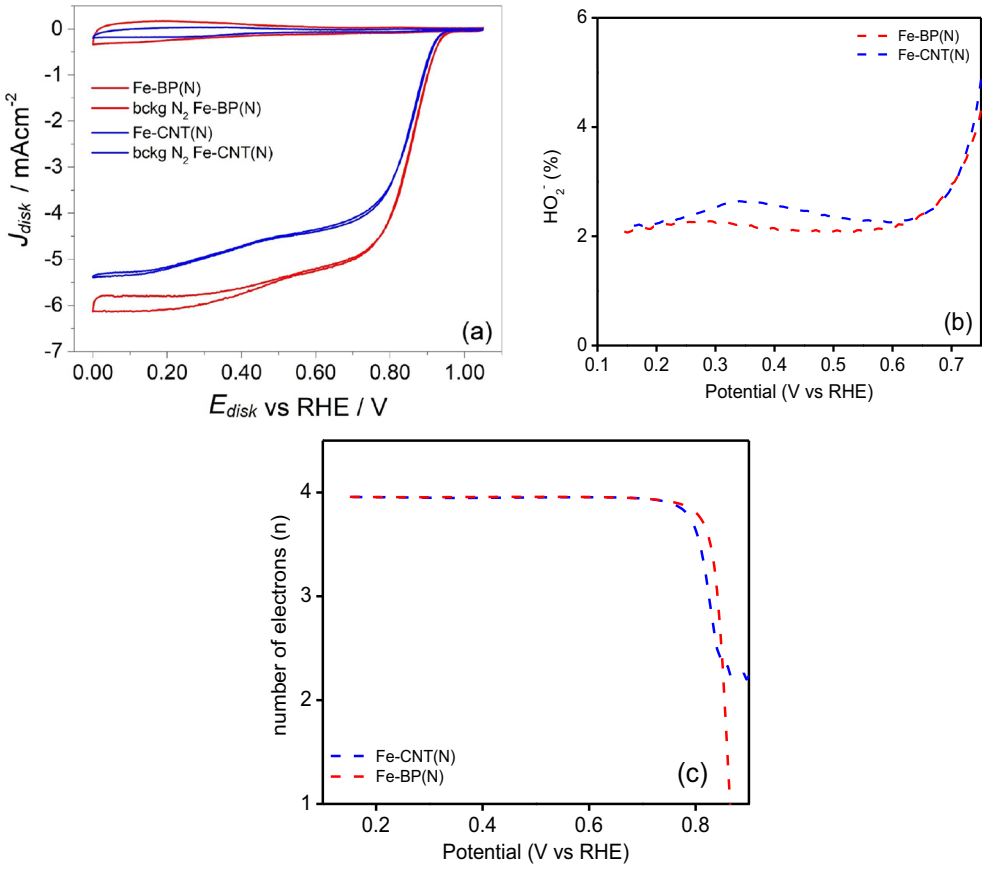

Fig. 4 **a** LSV of catalysts (5 mVs^{-1}, 1600 rpm) in O_2-saturated 0.1 M KOH. **b** Peroxide percentage generated by the catalyst over the entire potential range. **c** Number of electrons transferred in the ORR kinetics for the catalyst

The Fe-macrocycle on carbon black pearls and carbon nanotubes exhibits very similar performance in terms of onset potential, half-wave potential, limiting current, and electrons transfer pathway. This similar electrochemical behavior can be attributed to the use of FePc on the surface of carbon support. That is, the role of carbon support consists specially on the improvement of active sites, in the keep stick open the Fe-macrocycle and avoiding the aggregation phenomena typical of FePc without support [79, 83, 86, 87]. In addition, other characteristic of carbon support to facilitate the electrochemical performance of composites is the presence of N-functionalities and high structural defects and conductivity, in terms of charge dispersion, stability through the π-π interaction, and increasing overpotential ORR [34, 56, 65, 66].

Several studies were discussed previously considering Fe-based electrocatalysts with different architecture to oxygen reduction in alkaline media. Zhang et al. used FePc dispersed on 3D hierarchically porous carbon. These pyrolytic composites have a content of pyridinic nitrogen 87% and a $E_{1/2}$ of 0.89 V vs RHE, while our Fe-BP(N) and Fe-CNT(N) have a 62.2% and 47.4% of pyridinic N content with a correspondent $E_{1/2}$ of 0.84 V vs RHE. The comparison between the Fe-N-C catalysts indicate a similar potential for all catalysts with a range of 0.05 V and the performance here reported are slightly lower, this mainly due to the higher content of pyridinic N equivalent to 40–25% that influencing to create more active sites and enhance ORR [65]. As extensively studied and discussed, N-dopants modify the surface chemistry and local electronic properties enhancing the ORR rate. So that, N-doped carbon enable the synergism with Fe-macrocycle active sites toward higher ORR performance [87, 88]. In fact, high temperature pyrolyzed FePc/N-doped graphene contained a pyridinic N content of 88%, higher than our materials but with electrochemical performance very close to 0.86 V vs RHE. The high porous defect of Fe-BP(N) and Fe-CNT(N) high electrical conductivity, probably contributed for the similar ORR performance of catalyst. Furthermore, the N-rich coordination structure in FePc with carbon facilitates the tuning coordination environment of Fe atoms during pyrolysis. In this case, our catalysts take advance due to fact that non-pyrolysed method was used [56]. Recent workers used Fe-porphyrin over carbon Vulcan after pyrolysis and their pyridinic N content is 42% with a $E_{1/2}$ of 0.71 V vs. RHE. The performance here reported are slightly higher than the catalysts presented in that work [46, 73].

Transition metal oxide with FePc on graphene have exhibited $E_{1/2}$ of 0.88, 0.86, 0.85 V vs. RHE for FeO_x/FePc, CoO_x/FePc, and NiO_x/FePc respectively. It is notable that the half-wave potential of the TMO/FePc-graphene composites is higher when FeO_x in present compared to the others TMO. However, the enhancing oxygen reduction activity very similar to the samples can be attributed to the synergistic effect of the ultrafine TMO assist the ORR on FePc-graphene and to nanostructured carbon substrates CNT(N) and BP(N) [35].

Raman spectroscopy gave information on the structure and topologies of Fe-BP(N) and Fe-CNT(N). Results show both D and G bands at 1353 cm^{-1} and 1593 cm^{-1} respectively. As previously reported, the D band is associated with structural defects and G the G band corresponds to the E2g vibration mode Sp2 carbon domains. ID:IG ratio is proportional to the degree of defect sites in the carbon structure. Thereby, the ID:IG relative intensity ratio of both materials is 1.04 and 0.73 respectively. As shown in literature, Qiu et al. synthesized a FePc-graphene nanospheres with an ID:IG ratio of 0.88 and corresponding of 0.86 V vs RHE. Li and co-works developed a FePc macrocycle onto three different carbon supports: graphene oxide, mesoporous carbon vesicle, and ordered mesoporous carbon both display two eminent peaks at 1355, 1592 cm^{-1}, 1343 and 1590 cm^{-1} and 1345, 1598 cm^{-1} of D and G band respectively, with an ID:IG relative intensity ratio of 1.44, 1.74, and 1.93 with a $E_{1/2}$ of 0.83, 0.86, and 0.89 V vs RHE. Here, results suggest that highest intensity ratio is correlated to the presence of more edge plane-like defective sites of the material and may provide more anchoring sites for ORR. In this view, Raman results of composites confirm an interaction between FePc and carbon support originating from the G band of carbon materials.

A shift of G band of Fe-composite with respect to carbon support indicates the activity of nitrogen active sites in the interaction improvement of Fe-macrocycle/support via π-π stacking interaction [41, 84]. The previous FePc anchored in different carbon materials has very similar results in terms of electrochemical, even when the structural defects are higher. Functionalized multi-walled carbon nanotubes with FePc have a half-wave potential the same to our catalyst [52]. The above discussion comparing different FePc-based carbon materials clearly shown that in alkaline media, these catalysts have a very similar electrochemical performance even when the chemical and structural morphology were different. In addition, all of results are in accordance when our composite possesses a superior ORR activity to commercial Pt/C catalyst [52, 56, 65]. Particularly, Fe-BP(N) and Fe-CNT(N) may exhibit competitive or even better oxygen reduction activity in basic pH with positive onset potential, half-wave potential in comparison with previously reported FePc-based catalysts.

Conclusion

A recent literature overview on Fe-phthalocyanine supported on carbonaceous support is presented. Particularly, in this work, we describe the non-pyrolytic synthesis of two high-performance supported oxygen reduction catalysts using different carbon-based supports, carbon nanotubes, and black pearls (spherical carbon nanoparticles). The active catalytic material on both these supports is iron(II) phthalocyanine. Catalytic properties for both catalysts are quite similar because

of the similarity in surface chemistry and surface area of the materials. The cause for some differences in activity is the morphology and structure of the support materials that has been explored in this article. The Fe-BP(N) exhibits higher defect density in the structure which is a contributing factor toward enhanced oxygen reduction. However, the higher conductivity of carbon nanotube support in Fe-CNT(N) enhances electron transport and generates a slightly higher half-wave potential for ORR in alkaline electrolyte.

References

1. Thompson ST, James BD, Huya-Kouadio JN, Cassidy Houchin C, Daniel A, De Santis DA, Rajesh Ahluwalia R, Wilson AR, Kleen G, Papageorgopoulos D (2018) Direct hydrogen fuel cell electric vehicle cost analysis: system and high-volume manufacturing description, validation, and outlook. J Power Sources 399:304–313
2. Ralph TR, Hogarth MP (2002) Catalysis for low temperature fuel cells. Part I: the cathode challenges. Platin Met Rev 46:117–135
3. Song C, Zhang J (2008) Electrocatalytic oxygen reduction reaction. In: Zhang J (ed) PEM fuel cell electrocatalysts and catalyst layers. Springer, London. https://doi.org/10.1007/978-1-84800-936-3_2
4. Kinoshita K, Electrochemical society, electrochemical oxygen technology, Wiley, 1992, https://www.wiley.com/en-us/Electrochemical+Oxygen+Technology-p 978–0–471-57043-1]
5. Chen Y, Artyushkova K, Rojas-Carbonell S, Serov A, Matanovic I, Santoro C, Asset T, Atanassov P (2018) Inhibition of surface chemical moieties by tris(hydroxymethyl) aminomethane: a key to understanding oxygen reduction on iron–nitrogen–carbon catalysts. ACS Appl Energy Mater 1:1942–1949
6. Tylus U, Jia Q, Hafiz H, Allen RJ, Barbiellini B, Bansil A, Mukerjee S (2016) Engendering anion immunity in oxygen consuming cathodes based on Fe-Nx electrocatalysts: spectroscopic and electrochemical advanced characterizations. Appl Catal B Environ 198:318–324
7. Yang W, Li J, Lan L, Fu Q, Zhang Z, Zhu X, Liao Q (2018) Poison tolerance of non-precious catalyst towards oxygen reduction reaction. Int J Hydrog Energy 43:8474–8479
8. Minachev KM, Shuikin NI, Rozhdestivenskaya ID (1952) Poisoning of platinum catalysts with a low content of active metal on a carrier, under conditions of dehydrogenation catalysis. B Acad Sci 1:567–575
9. Reshetenko TV, Bethune K, Rubio MA, Rocheleau R (2014) Study of low concentration CO poisoning of Pt anode in a proton exchange membrane fuel cell using spatial electrochemical impedance spectroscopy. J Power Sources 269(2014):344–365
10. Reshetenko TV, St-Pierre J (2015) Study of acetylene poisoning of Pt cathode on proton exchange membrane fuel cell spatial performance using a segmented cell system. J. Power Sources 287:401–415
11. Reshetenko TV, St-Pierre J (2015) Study of the acetonitrile poisoning of platinum cathodes on proton exchange membrane fuel cell spatial performance using a segmented cell system. J Power Sources 293:929–940
12. Thompson S (2018) Direct hydrogen fuel cell electric vehicle cost analysis: system and high-volume manufacturing description, validation, and outlook. J Power Sources 399:304–313
13. Setzler BP, Zhuang Z, Wittkop JA, Yan Y (2016) Activity targets for nanostructured platinum-group-metal-free catalysts in hydroxide exchange membrane fuel cells. Nat Nanotechnol 11(12):1020–1025
14. Lefèvre M, Proietti E, Jaouen F, Dodelet JP (2009) Iron-based catalysts with improved oxygen reduction activity in polymer electrolyte fuel cells. Science 324(5923):71–74
15. Jaouen F, Proietti E, Lefèvre M, Chenitz R, Dodelet JP, Wu G, Chung HT, Johnston CM, Zelenay P (2011) Recent advances in non-precious metal catalysis for oxygen-reduction reaction in polymer electrolyte fuel cells. Energy Environ Sci 4:114–130
16. Artyushkova K, Serov A, Rojas-Carbonell S, Atanassov P (2015) Chemistry of multitudinous active sites for oxygen reduction reaction in transition metal-nitrogen-carbon electrocatalysts. The J Phys Chem C 119:25917–25928
17. Olson TS, Pylypenko S, Fulghum JE, Atanassov P (2010) Bifunctional oxygen reduction reaction mechanism on non-platinum catalysts derived from pyrolyzed porphyrins. J Electrochem Soc 157:54–63
18. Venegas R, Zagal JH, Kruusenberg I, Tammeveski K, Recio J, Muñoz K (2017) Oxygen reduction on carbon-supported metallophthalocyanines and metalloporphyrins. Elsevier Encyclopedia of Interfacial Chemistry and Electrochemistry 812-819
19. Zagal JH, Fethi B (Eds.) electrochemistry of N4 macrocyclic metal complexes. Volume 1: energy. Springer
20. Zagal JH, Koper MTM (2016) Reactivity descriptors for the activity of molecular MN4 catalysts for the oxygen reduction reaction. Angew Chemi Int 55:14510–14521
21. Abarca B, Viera M, Aliaga C, Marco JF, Orellana W, Zagal JH, Tasca F (2019) In search of the most active MN4 catalyst for the oxygen reduction reaction. The case of perfluorinated Fe phthalocyanine. J Mater Chem A 7:24776–24783
22. Kimura M, Kuroda T, Ohta K, Hanabusa K, Shirai H, Kobayashi N (2003) Self-organization of hydrogen-bonded optically active phthalocyanine dimers. Langmuir 19:4825–4830
23. Dong G, Huang M, Guan L (2012) Iron phthalocyanine coated on single-walled carbon nanotubes compositefor the oxygen reduction reaction in alkaline mediaw. Phys Chem Chem Phys 14(8):2557–2559
24. Alsudairi A, Li J, Ramaswamy N, Mukerjee S, Abraham KM, Jia Q (2017) Resolving the iron phthalocyanine redox transitions for ORR catalysis in aqueous media. J Phys Chem Lett 8:2881–2886
25. Van Den Brink F, Visscher W, Barendrecht E (1984) Electrocatalysis of cathodic oxygen reduction by metal phthalocyaninesn. Part III. Iron phthalocyanine as electrocatalyst: experimental part. J Elecrroanal Chem 172:301–325
26. Zagal JH, Pgez M, Tanaka AA, Santos JR, Linkous CA (1992) Electrocatalytic activity of metal phthalocyanines for oxygen reduction. J Ekctroanal Chem 339:13–30
27. Zagal JH, Griveau S, SilvA JF, Nyokong T, Bedioui F (2010) Metallophthalocyanine-based molecular materials as catalysts for electrochemical reactions. Coord Chem Rev 254:2755–2791
28. Wu K-H, Shi W, Wang D, Xu J, Ding Y, Lin Y, Qi W, Zhang B, Su D (2017) In situ electrostatic modulation of path selectivity for the oxygen reduction reaction on Fe−N doped carbon catalyst. Chem Mater 29:4649–4653
29. Zhang Z, Dou M, Ji J, Wang F (2017) Phthalocyanine tethered iron phthalocyanine on graphitized carbon black as superior electrocatalyst for oxygen reduction reaction. Nano Energy 34:338–343
30. Cui L, Lv G, Dou Z, He X (2013) Fabrication of iron phthalocyanine/graphene micro/nanocomposite by solvothermally assisted π–π assembling method and its application for oxygen reduction reaction. Electrochim Acta 106:272–278
31. Taniguchi T, Tateishi H, Miyamoto S, Hatakeyama K, Ogata C, Funatsu A, Hayami A, Makinose Y, Matsushita N, Koinuma M, Matsumoto Y (2013) A self-assembly route to an iron

phthalocyanine/reduced graphene oxide hybrid electrocatalyst affording an ultrafast oxygen reduction reaction. Part Part Syst Charact 30:1063–1070
32. Jiang Y, Yizhong L, Lv X, Han D, Zhang Q, Niu L, Chen W (2013) Enhanced catalytic performance of Pt free iron phthalocyanine by graphene support for efficient oxygen reduction reaction. ACS Catal 3:1263–1271
33. Zhang C, Hao Z, Yin H, Liu H, Hou L (2012) Iron phthalocyanine and nitrogen-doped graphene composite as a novel non-precious catalyst for the oxygen reduction reaction. Nanoscale 4:7326–7329
34. Komba N, Zhang G, Wei Q, Yang X, Prakash J, Chenitz R, Rosei F, Sun S (2019) Iron (II) phthalocyanine/N-doped graphene: a highly efficient non-precious metal catalyst for oxygen reduction. Int J Hydrog Energy 44:18110–18114
35. Cheng Y, Wu X, Veder J-P, Thomsen L, Jiang S-P, Wang S (2019) Tuning the electrochemical property of the ultrafine metal-oxide nanoclusters by iron phthalocyanine as efficient catalysts for energy storage and conversion. Energy Environ Mater 2:5–17
36. Li M, Bo X, Zhang Y, Han C, Guo L (2014) Comparative study on the oxygen reduction reaction electrocatalytic activities of iron phthalocyanines supported on reduced graphene oxide, mesoporous carbon vesicle, and ordered mesoporous carbon. J Power Sources 264:114–122
37. Liu Y, Wu Y-Y, Lv G-J, Pu T, He X-Q, Cu L-L (2013) Iron (II) phthalocyanine covalently functionalized graphene as a highlyefficient non-precious-metal catalyst for the oxygen reduction reaction in alkaline media. Electrochim Acta 112:269–278
38. Zhang Y, Qian L, Zhao W, Li X, Huang X, Mai X, Wang Z, Shao Q, Yan X, Guo Z (2018) Highly efficient Fe-N-C nanoparticles modified porous graphene composites for oxygen reduction reaction. J Electrochem Soc 165:H510–H516
39. Ohtsuka M, kitamura F (2015) On the formal redox potential of oxygen reduction reaction at iron phthalocyanine/graphene composite electrode in alkaline media. Electrochemistry 83: 376–380
40. Taniguchi T, Tateishi H, Miyamoto S, Hatakeyama K, Ogata K, Funatsu A, Hayami S, Makinose Y, Matsushita N, Koinuma M, Matsumoto Y (2013) A self-assembly route to an iron phthalocyanine/reduced graphene oxide hybrid electrocatalyst affording an ultrafast oxygen reduction reaction. Particle 30: 1063–1070
41. Qiu X, Yan X, Pang H, Wang J, Sun JD, Wei S, Xu L, Tang Y (2018) Isolated Fe single atomic sites anchored on highly steady hollow graphene nanospheres as an efficient electrocatalyst for the oxygen reduction reaction. Adv Sci 6:1801103
42. Nabae Y, Moriya S, Matsubayashi K, Lyth JM, Malon M, Wu L, Islam NM, Koshigoe W, Kuroki S, Kakimoto MA, Miyata S, Ozaki JI (2010) The role of Fe species in the pyrolysis of Fe phthalocyanine and phenolic resin for preparation of carbon-based cathode catalysts. Carbon 48:2613–2624
43. Miller AH, Bellini M, Oberhauser W, Deng X, Chen H, He Q, Passaponti M, Innocenti M, Yang R, Sun F, Jiang Z, Vizza F (2016) Heat treated carbon supported iron (II) phthalocyanine oxygen reduction catalysts: elucidation of the structure-activity relationship using X-ray absorption spectroscopy. Phys Chem Chem Phys 18(48):33142–33151
44. Chung DY, Kim MJ, Kang N, Yoo JM, Shin H, Kim O-H, Sung Y-E (2017) Low-temperature and gram-scale synthesis of two-dimensional Fe-N-C carbon sheets for robust electrochemical oxygen reduction reaction. Chem Mater 29:2890–2898
45. Zagal JH, Recio FJ, Gutierrez CA, Zuñiga C, Páez MA, Claudia A (2014) Caro towards a unified way of comparing the electrocatalytic activity MN_4 macrocyclicmetal catalysts for O_2 reduction on the basis of the reversible potential of the reaction. Electrochem Commun 41:24–26
46. Zuniga C, Candia-Onfray C, Venegas R, Munoz K, Urra J, Sanchez-Arenillas M, Marco JF, Zagal JH, Recio FJ (2019) Elucidating the mechanism of the oxygen reduction reaction for pyrolyzed Fe-N-C catalysts in basic media. Electrochem Commun 102:78–82
47. Monteverde Videla AHA, Osmieri L, Specchia S (2016) Non-noble metal (NNM) catalysts for fuel cells: tuning the activity by a rational step by step single variable evolution. In: Bedioui F, Zagal JH (eds) Electrochemistry of N4 macrocyclic metal complexes. Springer International Publishing AG, Switzerland, pp 69–101
48. Alessandro HA, Monteverde V, Osmieri L, Armandi M, Specchia S (2015) Varying the morphology of Fe-N-C electrocatalysts by templating iron phthalocyanine precursor with different porous SiO_2 to promote the oxygen reduction reaction. Electrochim Acta 177:43–50
49. Osmieri L, Alessandro HA, Monteverde V, Armandi M, Specchia S (2016) Influence of different transition metals on the properties of Me-N-C (Me = Fe, Co, Cu, Zn) catalysts synthesized using SBA-15 as tubular nano-silica reactor for oxygen reduction reaction. Int J Hydrog Energy 41:22570–22588
50. Alessandro HA, Monteverde V, Sebastian D, Vasile NS, Osmieri L, Arico AS, Baglio V, Specchia S (2016) Performance analysis of Fe-N-C catalyst for DMFC cathodes: effect of water saturation in the cathodic catalyst layer. Int J Hydrog Energy 47:22605–22618
51. Osmieri L, Escudero-Cid R, Alessandro HA, Monteverde V, Ocón P, Specchia S (2018) Application of a non-noble Fe-N-C catalyst for oxygen reduction reaction in an alkaline direct ethanol fuel cell. Renew Energy 115:226–237
52. Yan X, Xu X, Liu Q, Guo J, Kang L, Yao J (2018) Functionalization of multi-walled carbon nanotubes with iron phthalocyanine via a liquid chemical reaction for oxygen reduction in alkaline media. J Power Sources 389:260–269
53. Yang J, Toshimitsu F, Yang Z, Fujigaya T, Nakashima N (2017) Pristine carbon nanotube/iron phthalocyanine hybrids with a well-defined nanostructure show excellent efficiency and durability for oxygen reduction reaction. J Mater Chem A 5:1184–1191
54. Dong G, Huang M, Guan L (2012) Iron phthalocyanine coated on single-walled carbon nanotubes composite for the oxygen reduction reaction in alkaline media. Phys Chem Chem Phys 14(8):2557–2559
55. Cañete P, Silva JF, Zagal JH (2014) Electrocatalytic activity for O_2 reduction of unsubstituted and perchlorinated iron phthalocyanines adsorbed on amino-terminated multiwalled carbon nanotubes deposited on glassy carbon electrodes. J Chil Chem Soc 59:2
56. Venegas R, Recio FJ, Zuniga C, Viera M, Oyarzun M-P, Silva N, Neira F, Marco JF, Zagal JH, Tasca F (2017) Comparison of the catalytic activity for O_2 reduction of Fe and Co MN_4 adsorbed on graphite electrodes and on carbon nanotubes. Phys Chem Chem Phys 19:20441–20450
57. Kim D-H, Kwak D-H, Han S-B, Park H-S, Park J-Y, Won J-E, Ma K-B, Yun S-H, HuiKwon S, Koh MK, Park K-W (2018) The role of arginine as nitrogen doping and carbon source for enhanced oxygen reduction reaction. Int J Hydrog Energy 43:1479–1488
58. Jiang WJ, Gu L, Li L, Zhang Y, Zhang X, Zhang L-J, Wang J-Q, Hu J-S, Wei Z, Wan L-J (2016) Understanding the high activity of Fe-N-C electrocatalysts in oxygen reduction: Fe/Fe3C nanoparticles boost the activity of Fe-Nx. J Am Chem Soc 138(10):3570–3578
59. Daems N, Sheng X, Alvarez-Gallego Y, Vankelecoma IFJ, Pescarmona PP (2016) Iron-containing N-doped carbon electrocatalysts for the cogeneration of hydroxylamine and electricity in a H2–NO fuel cell. Green Chem 18:1547–1559
60. Yang D-S, Song MY, Singh KP, Yu J-S (2015) The role of iron in the preparation and oxygen reduction reaction activity of nitrogen-doped carbon. Chem Commun 51(12):2450–2453
61. Zhang Z, Dou M, Ji J, Waing F (2017) Phthalocyanine tethered iron phthalocyanine on graphitized carbon black as superior electrocatalyst for oxygen reduction reaction. Nano Energy 34: 338–343

62. Liu Y, Fan Y-S, Liu Z-M (2019) Pyrolysis of iron phthalocyanine on activated carbon as highly efficient non-noble metal oxygen reduction catalyst in microbial fuel cells. Chem Eng J 361:416–427
63. Saputro AG, Kasai H (2015) Oxygen reduction reaction on neighboring Fe–N_4 and quaternary-N sites of pyrolized Fe/N/C catalyst. Phys Chem Chem Phys 17(5):3059–3071
64. González EA, Gulppi Z, Páez MA, Zagal JH (2016) O_2 reduction on electrodes modified with nitrogen doped carbon nanotubes synthesized with different metal catalysts. Diam Relat Mater 64:119–129
65. Zhang Z, Sun J, Wang F, Dai L (2018) Efficient oxygen reduction reaction (ORR) catalysts based on single Iron atoms dispersed on a hierarchically structured porous carbon framework. Angew Chem 57:9038–9043
66. Ao X, Zhang W, Li Z, Lv L, Ruan Y, Wu H-H, Chiang W-H, Wang C, Liue M, Zeng XC (2019) Unraveling the high-activity nature of Fe-N-C electrocatalysts for oxygen reduction reaction: the extraordinary synergy between Fe-N_4 and Fe_4N. J Mater Chem A 7: 11792–11801
67. Chen M, He Y, Spendelow JS, Wu G (2019) Atomically dispersed metal catalysts for oxygen reduction. ACS Energy Lett 4:1619–1633
68. Zhanga H, Osgooda H, Xie XH, Shao Y, Wua G (2017) Engineering nanostructures of PGM-free oxygen-reduction catalysts using metal-organic frameworks. Nano Energy 31:331–350
69. Huang X, Yang Z, Dong B, Wang Y, Tang T, Hou Y (2017) *In-situ* Fe_2N@N-doped porous carbon hybrids as superior catalysts for oxygen reduction reaction. Nanoscale 9(24):8102–8106
70. Jiao L, Wan G, Zhang R, Zhou H, Yu S-H, Jiang H-L (2018) From metal–organic frameworks to single-atom Fe implanted N-doped porous carbons: efficient oxygen reduction in both alkaline and acidic media. Angew Chem Int Ed 57:1–6
71. Wang Y, Wang M, Zhang Z, Wang Q, Jiang Z, Lucero M, Zhang X, Li X, Gu M, Feng Z, Liang Y (2019) Phthalocyanine precursors to construct atomically dispersed iron electrocatalysts. ACS Catal 9: 6252–6626
72. Wang S, Li F, Wang F, Qiao D, Sun C, Liu J (2018) A superior oxygen reduction reaction electrocatalyst based on reduced graphene oxide and iron (II) phthalocyanine-supported Sub-2 nm platinum nanoparticles. ACS Appl Nano Mater 1:711–721
73. Praats R, Kruusenberg I, Käärik M, Joost U, Aruvälic J, Paiste P, Saar P, Rauwel P, Kook M, Leis J, Zagal JH, Tammeveski K (2019) Electroreduction of oxygen in alkaline solution on iron phthalocyanine modified carbide-derived carbons. Electrochim Acta 299: 999–1010
74. Seo MH, Higgins D, Jiang G, Choi SM, Han B, Chen Z (2014) Theoretical insight into highly durable iron phthalocyanine derived non-precious catalysts for oxygen reduction reactions. J Mater Chem A 2:19707–19716
75. Mussell S, Choudhury P (2016) Density functional theory study of iron phthalocyanine porous layer deposited on graphene substrate: a Pt-free electrocatalyst for hydrogen fuel cells. J Phys Chem C120: 5384–5391
76. Cao R, Thapa R, Kim H, Xu X, Gyu Kim M, Li Q, Park N, Liu M, Cho J (2013) Promotion of oxygen reduction by a bio-inspired tethered iron phthalocyanine carbon nanotube-based catalyst. Nat Commun 4:2076
77. Torre B, Svec M, Hapala P, Redondo J, Krejcí O, Lo R, Manna D, Sarmah A, Nachtigallová D, Tuček J, Błoński P, Otyepka M, Zboril M, Hobza P, Jelínek P (2018) Non-covalent control of spin-state in metal-organic complex by positioning on N-doped graphene. Nat Commun 9:2831
78. Hu X, Xia D, Zhang L, Zhang J (2013) High crystallinity binuclear iron phthalocyanine catalyst with enhanced performance for oxygen reduction reaction. J Power Sources 231:91–96
79. Wang X, Wang B, Zhong J, Zhao F, Han N, Huang W, Zeng M, Fan J, Li Y (2016) Iron polyphthalocyanine sheathed multiwalled carbon nanotubes: a high-performance electrocatalyst for oxygen reduction reaction. Nano Res 9:1497–1506
80. Santoro C, Gokhale R, Mecheri B, D'Epifanio A, Licoccia S, Serov A, Artyushkova K, Atanassov P (2017) Design of iron (II) phthalocyanine-derived oxygen reduction electrocatalysts for high-power-density microbial fuel cells. ChemSusChem 10:3243–3251
81. Yin X, Chung HT, Martinez U, Lin L, Artyushkova K, Zelenay P (2019) PGM-free ORR catalysts designed by templating PANI-type polymers containing functional groups with high affinity to Iron. J Electrochem Soc 166:F3240–F3245
82. Frackowiak E (2007) Carbon materials for supercapacitor application. Phys Chem Chem Phys 15:1774
83. Raggio M, Mecheri B, Nardis S, D'Epifanio A, Licoccia S, Paolesse R (2019) Metallo-Corroles supported on carbon nanostructures as oxygen reduction electrocatalysts in neutral media. Eur J Inorg Chem 44:4760–4765
84. Alsudairi A, Li J, Ramaswamy N, Mukerje S, Abraham KM, Jia Q (2017) Resolving the iron phthalocyanine redox transitions for ORR catalysis in aqueous media. J Phys Chem Lett 8(13):2881–2886
85. Zhao X, Zou X, Yan X, Brown CL, Chen Z, Zhu G, Yao X (2016) Defect-driven oxygen reduction reaction (ORR) of carbon without any element doping. Inorg Chem Front 3:417–421
86. Wang Y, Alsmeyer DC, McCreery RL (1990) Raman spectroscopy of carbon materials: structural basis of observed spectra. Chem Mater 2:557–563
87. Mecheri B, Ficca VCA, Oliveira MAC, D'Epifanio A, Placidi E, Arciprete F, Licoccia F (2018) Facile synthesis of graphene-phthalocyanine composites as oxygen reduction electrocatalysts in microbial fuel cells. Appl Catal B-Environ 237:699–707
88. Ning X, Li Y, Ming J, Wang Q, Wang H, Cao Y, Peng F, Yang Y, Yu H (2019) Electronic synergism of pyridinic- and graphitic-nitrogen on N-doped carbons for the oxygen reduction reaction. Chem Sci 10(6):1589–1596